

**MEMS-Based Optical Switch Design
for Reconfigurable, Fault-Tolerant
Optical Backplanes**

**N.R. Jankowski, C. Bobcowski,
D. Zipkin, R.R. Krchnavek,
and R.D. Chamberlain**

N.R. Jankowski, C. Bobcowski, D. Zipkin, R.R. Krchnavek, and R.D. Chamberlain, "MEMS-Based Optical Switch Design for Reconfigurable, Fault-Tolerant Optical Backplanes," in *Proc. of the 6th Int'l Conf. on Parallel Interconnects*, October 1999, pp. 149-156.

Rowan University
and
Washington University

MEMS-Based Optical Switch Design for Reconfigurable, Fault-Tolerant Optical Backplanes

Nicholas R. Jankowski, Christopher Bobcowski,
David Zipkin, and Robert R. Krchnavek
Rowan University
Glassboro, New Jersey

Roger D. Chamberlain
Washington University
St. Louis, Missouri

Abstract

One of the critical components in developing reconfigurable, fault-tolerant optical backplanes is a low-cost optical switch. Microelectromechanical systems (MEMS) are a strong candidate for fabricating a low-cost optical switch. In this paper, we discuss the design issues for such a switch. Furthermore, using the material discussed in this report, we have designed a complete MEMS-based optical switch. It was submitted for prototype manufacturing in May 1999.

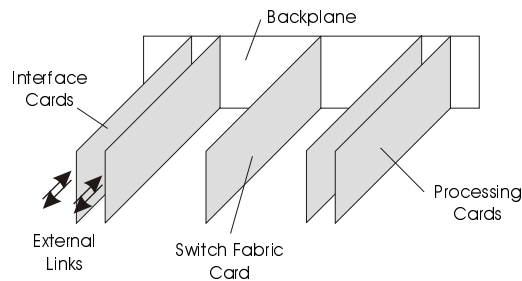


Figure 1. Backplane interconnect for a digital system.

1. Introduction

The prototypical interface technology used in tightly-coupled systems is the backplane. It is commonly used for the integration of board-level subsystems into a larger system. This is illustrated in Figure 1, which shows an embedded processing system that contains a number of interface cards (providing I/O functions), a card that implements a switch fabric, and several processing cards. These cards are interconnected with a board that delivers signals between the attached cards. While historically these systems were bus-based (e.g., VME), the need for increased performance has led to most systems incorporating a switched interconnect (e.g., SCI, Mercury Computer Systems' RACEway), hence the inclusion of the switch fabric card.

A nearly identical illustration can be used to describe a switching system for telecommunications networks. Here, the interface cards represent line cards, an ATM (Asynchronous Transfer Mode) switch fabric is in the center of the figure, and the processing cards are not present. In this system, although the detailed functions implemented by the attached cards are significantly different than the first example, the function

performed by the backplane interconnect is identical, delivery of high-speed signals from one card to another.

As described above, the backplane provides a set of passive point-to-point connections, with active switching taking place on one (or more) of the installed cards. This system-level interconnection technique provides a number of technical and economic advantages. System repair is simplified since cards can be easily replaced. System expansion can be supported via empty slots. System upgrades are also straightforward via card replacement. As a result, backplane-based systems are pervasive in the digital systems arena, for an extremely wide variety of designs. With the push to ever higher data rates, designers are looking to optics for improved interconnect bandwidth, and a number of passive optical fiber-based backplane systems have been constructed (e.g., AT&T Monet [1]).

An additional technical challenge associated with backplane designs is the need to provide for fault-tolerant, reconfigurable systems. By *fault tolerance* we mean the ability of the system to keep operating in the presence of a faulty component (or subsystem). Generally faults, once detected and identified, are dealt with

by replacing faulty components with nonfaulty components (i.e., spares already installed in the backplane).

While interchange of components for fault tolerance generally maintains system functionality, we refer to *reconfiguration* as component changes which alter functionality. DoD is actively supporting the design of systems with this capability through the DARPA Adaptive Computing Systems program [2], where reconfigurable processing nodes are to be tied together with a reconfigurable interconnect. In a telecommunications environment, fast reconfigurability provides the ability to perform dynamic load balancing. That is, depending on the load associated with individual connections, certain resources (i.e., line cards and fiber links) can be reassigned in real time so that sufficient bandwidth is made available to heavily loaded communication paths.

Additionally, it is often necessary to reconfigure systems when new components are manually added or removed from the system. This typically occurs in a system upgrade situation. The ability to easily reconfigure the backplane to support the upgrade can be a significant benefit.

We can provide for fault-tolerance and reconfiguration by designing a backplane where the point-to-point optical links can be dynamically changed (i.e., switched). Here, we do not require fast switching, for example on a per message basis, but slow switching (e.g., ≤ 50 ms switching time). A key element required for such a design is a low-cost, small-size optical switch capable of switching a single input fiber between two output fibers. Here, we describe the design of an optical fiber switch constructed using microelectromechanical systems (MEMS) technology. This design can be produced at low cost and is capable of being integrated into an optical backplane.

Several optical switches have been fabricated using MEMS technology [3, 4, 5]. However, little has been published on using optical fiber as an integral part of the switch. The advantages of using optical fiber (lensless) switches are: greater alignment tolerance; simpler assembly; low optical loss; insensitivity to the characteristics of the signals being transmitted; and insensitivity to signal wavelength.

No assembly is the key to producing a low-cost optical switch. Our design satisfies this criteria. The prototypes are being fabricated using the MUMPs (Multi-User MEMS Process) process at Cronos Integrated Microsystems (formerly MCNC) in North Carolina. Other than the attaching of optical fibers to the completed product, MUMPs will be the only manufacturing step in the production of the device. The process will yield a working switch at an extremely low cost when compared to other existing optical switches cur-

rently on the market.

This paper describes several aspects of the switch, including the key elements of the design. We begin with a brief description of the switching device. Then, some background is given as to the nature of the task to be accomplished, i.e., the bending of an optical fiber. Next, the major device components are discussed in detail. Finally, some test structures that were included on the fabricated chip are discussed.

2. Switch Description

Figure 2 shows a schematic diagram of the optical switch. The moving end of the optical fiber is fixed to the slider piece. A pair of thermally actuated stepper motors, operated 180° out of phase, control the motion of the fiber. Using thermal actuation, these stepper motors cycle through a sequence of movements until the fiber has been moved from Output Fiber 1 to Output Fiber 2. There are no mechanisms holding the fiber in place in the initial (rest) position. For the time being, we felt it was sufficient to let the fiber's spring force hold itself in position when in the straight position. In the extended or bent position, a locking mechanism (latch) is used to hold the fiber in place. As one can readily see from Figure 2, this is not a simple switch design. In the paragraphs that follow, an explanation for the complexity will be provided, along with the design questions that were answered along the way.

3. Optical Fiber Analysis

Since this design will primarily focus on the movement of a single piece of optical fiber, we first consider the mechanical behavior of such a fiber. We decided to use $125 \mu\text{m}$ diameter multimode optical fiber in this design. Multimode fiber has a larger diameter core ($50 \mu\text{m}$) than does single-mode fiber ($10 \mu\text{m}$). This allows for much greater tolerances when aligning fibers during the switching process.

The optical fiber used will be arranged as shown in Figure 3. Initially, it will be aligned with one of the output fibers. Then, a force will be applied to the fiber, bending it into alignment with the other output fiber.

As can be seen in the sketch, as α approaches 0, i.e., as the output fibers are placed closer together, the total distance that needs to be traveled by the end of the fiber, δ , approaches the fiber diameter, d . Therefore, to minimize the travel distance, the two output fibers should be placed as close together as possible.

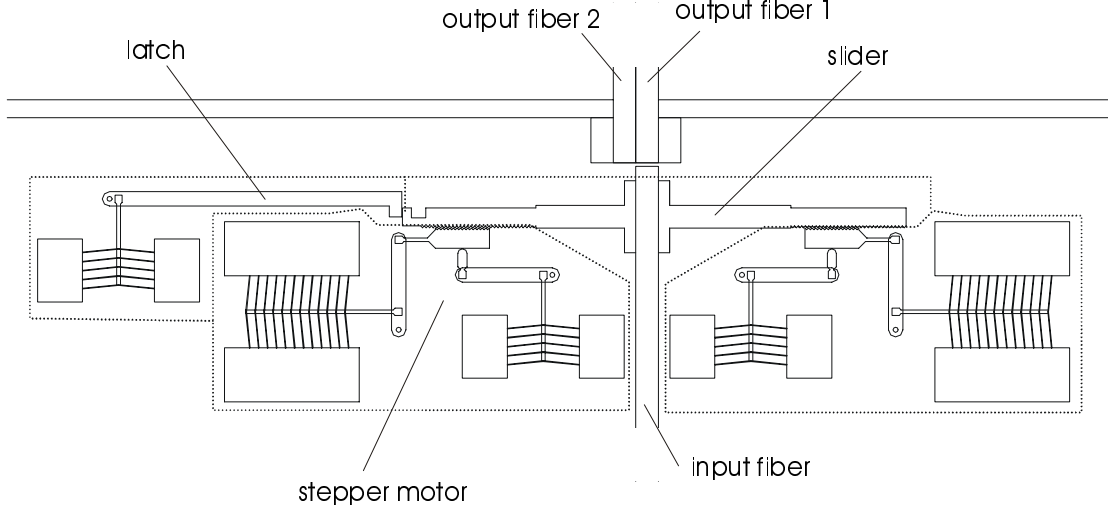


Figure 2. Schematic diagram of the MEMS-based optical switch.

3.1. Fiber Bending Calculations

The optical fiber can be modeled as a simple cantilever beam with a point load applied at the free end (Figure 3). Initially, we will assume that this force is constant. A force (P) needs to be applied to the fiber to move it sufficient distance to line up with the other output fiber. The displacement of the fiber end as a function of the applied force and the length of the cantilever is given by

$$y(L) = \frac{PL^3}{3EI} \quad (1)$$

where L is the length of the fiber, P is the applied force at L , E is the modulus of elasticity of the material, and I is the moment of inertia of the beam cross-section.

For the optical fiber that we will be using, E is 73 GPa, $y(L)$ can be assumed to be equal to the diameter (d) of the fiber ($125 \mu\text{m}$), and $I = \frac{1}{64}\pi d^4$. This leaves the applied force, P , and the active fiber length, L , as

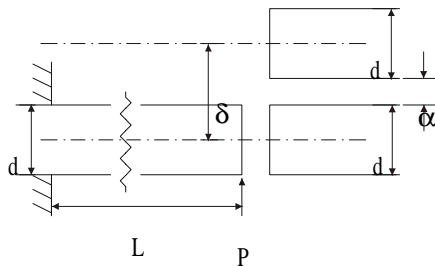


Figure 3. Schematic representation of the optical fiber dimensions.

the only two variables in equation (1), which becomes

$$P = \frac{3\pi d^5 E}{64L^3} \quad (2)$$

Figure 4 shows this relationship graphically. The graph

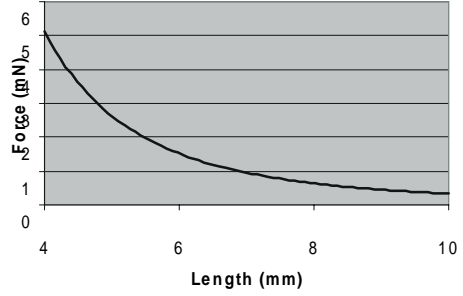


Figure 4. Fiber bending force plot.

shows a significant drop in the required force over the 4-10 mm range. MUMPS allows us to fabricate our device on a $1 \text{ cm} \times 1 \text{ cm}$ chip. Depending on the structure sizes in our design, we should have an active fiber length of about 9 mm. Using this value with equation (2) yields

$$P = 450 \mu\text{N}. \quad (3)$$

This is the force that our device will need to produce in order to complete the switch operation.

4. Switch Design

The primary consideration in this design is developing an actuator that can be used to successfully achieve

the required force/distance combination. The force of $450 \mu\text{N}$ and a displacement of $125 \mu\text{m}$ is an extremely large requirement for a MEMS based actuator. Some amplification method will have to be used to achieve the desired output. We will first describe the actuator type that we decided to use and then the amplifier and its components.

4.1. The Actuator

After some initial research, it was decided that thermal actuation should be used. The other mainstream option is electrostatic actuation, but so far, that has not been seen to be capable of achieving the forces applicable to our situation.

Direct thermal expansion, however, is not the answer. In MUMPS, the only structural material available is polysilicon. This material has a rather low coefficient of linear thermal expansion ($\approx 2.5 \text{ ppm}/^\circ\text{C}$). Therefore, the actuators themselves will have to be configured in such a way as to magnify their own force/displacement production.

Another consideration with thermal actuators is that the force created by such an actuator is not constant. The force is created by the induced thermal stress in the material. This stress is transformed into thermal strain until a new equilibrium position is reached. As a result, thermal force is inversely proportional to actuator deflection.

Figure 5 is a sketch of an in-plane, bent-beam actuator with fixed supports [6]. For a polysilicon bent-beam actuator with $L = 800 \mu\text{m}$, $\theta = 0.2 \text{ rad}$, width = $10 \mu\text{m}$, and thickness = $3.7 \mu\text{m}$, experiments have produced results such as that shown in Figure 6 [6]. In the study, force was calculated from displacement measurements using differential bent-beam analysis. As can be seen in the two graphs, this actuator type can produce a large force, but the displacement is significantly lower than what we required.

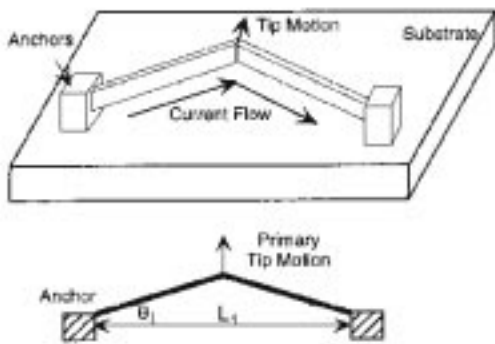


Figure 5. Bent-beam actuator design from [6]

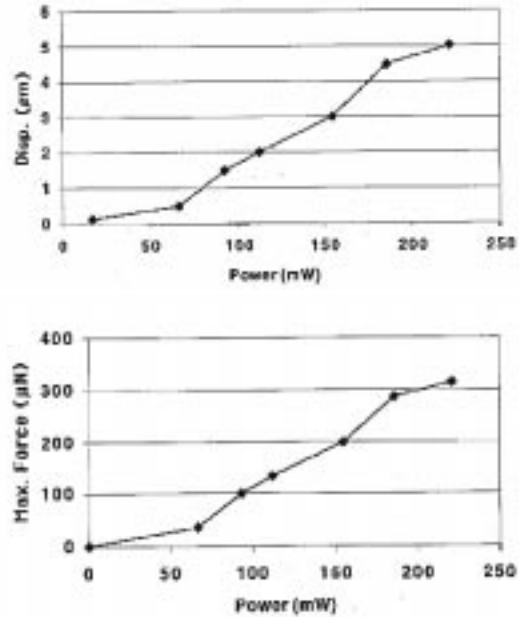


Figure 6. Bent-beam actuator displacement and calculated maximum force from [6].

Individually, these simple beam actuators do not quite meet the design need, but they can be combined in certain ways to enhance their overall performance. Connecting them in series (mechanically in series, electrically they are connected in parallel) will magnify their force output without modifying their deflection characteristics. In addition, these devices can be cascaded, with results much more impressive than for the single bent-beam actuator. However, cascading bent-beam actuators requires considerable real estate and power. It is likely that a properly designed cascade bent-beam actuator would have a better figure of merit than series connected bent-beam actuators. However, for simplicity, we have ruled them out for this design.

Finally, it should be noted that the bent-beam actuators analyzed in [6] were not optimized. Proper angular configuration could change the actuator performance as discussed by the authors. In our work, we have chosen an angle that produces a known force/displacement performance and included several test structures to study the effect of different bent-beam actuator geometries.

4.2. Amplification Methods

Because we are using an actuator with a deflection much less than our requirement, but a force (when multiple actuators are connected in series mechanically) much higher than our requirement, we can use me-

chanical amplification methods to reach the necessary deflection.

According to the bent-beam study [6], a bent-beam actuator with the geometry described above can produce a zero-force deflection of about $3 \mu\text{m}$, and a zero-deflection force of about $750\text{-}800 \mu\text{N}$. Note, for the MUMPS process, the zero-deflection force is approximately $600\text{-}650 \mu\text{N}$ for this design. Assuming we use $2/3$ of the full range displacement ($\approx 2 \mu\text{m}$), our output force will be $1/3$ of the total output force or $\approx 200 \mu\text{N}$. In order to achieve $125 \mu\text{m}$ motion with $450 \mu\text{N}$ output, we would need about $140\text{-}145$ of these actuators connected to a lever with a magnification of 62.5 . This is definitely not feasible for our design. However, the actuator could much more easily provide the needed force over smaller distances, such as $10\text{-}15 \mu\text{m}$. With this magnification in mind, for an output force of $450 \mu\text{N}$, we would need only $11\text{-}12$ actuators, with an amplification of 5 for the distance. This is a much more realistic number.

Since we can more easily move these smaller distances, we require multiple motions to achieve the total distance of $125 \mu\text{m}$. Thus, we have designed a *stepper motor* to accomplish the movement.

4.2.1 Stepper Motor Principles

The stepper motor uses a timed combination of a driving actuator (driver) and a clamping actuator (pusher). These motions are depicted in Figure 7. At rest, the driving actuator would not be in contact with the sliding piece to be moved (slider). At the start of the motion cycle, the pusher would clamp the driver against the slider. Then the driver would actuate, moving the slider in the desired direction. At full extension, the pusher would release the driver allowing it to pull back without being in contact with the slider. Thus the slider would maintain its position. The cycle is then repeated as often as is needed to obtain the required motion. Using this mechanism, several actuators are attached to the pusher and driver pieces, and the fiber is switched in this manner.

This method is more complicated than a method using direct actuator amplification. Issues such as cycle time, timing algorithms and intermediate clamping will need to be addressed when moving the fiber. However, given the available actuators, this seems to be the simplest means capable of performing the desired task. As such, we then must look into the design of the individual stepper motor components.

The stepper motor consists of thermal actuators, actuator connections, pins, levers, the slider, drive pawl, and latch. Refer to Figure 2 for the placement of these

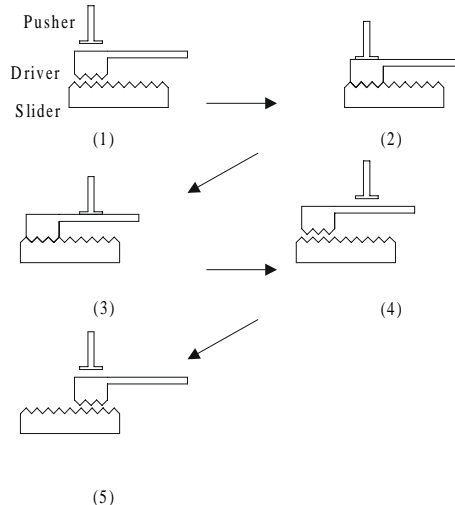


Figure 7. Stepper motor cycle.

components.

Actuators As mentioned previously, we are using bent-beam arrays. There are two main types of actuator arrays in the stepper design. The drive actuators are arrays of 12 beams connected in series (mechanically). Similarly configured, arrays of 5 beams are used for the pusher and lock mechanisms. The beam characteristics are $L = 400 \mu\text{m}$, $\theta = 0.1 \text{ rad}$, $w = 4 \mu\text{m}$, and $t = 3.5 \mu\text{m}$.

The base pads are designed with a large area to promote even current distribution to the beams. This large area also allows them to act as stable supports for the beams. Figure 8 shows a sketch of the driver actuator array.

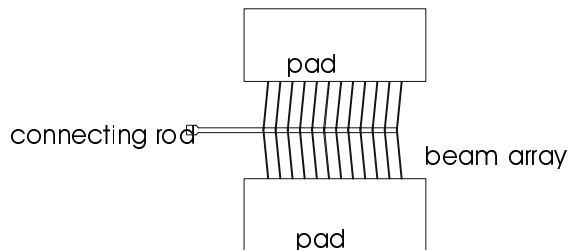


Figure 8. Driver actuator.

Actuator connections The actuators attach to the levers by a fixed connecting rod. We had originally wanted pin joint connections. This proved impractical for two reasons: (i) how to make a 1 degree of freedom pin joint with only a 3 structural layer process; and (ii) the MUMPS process required at least $2 \mu\text{m}$ spacing between individual

components on the same layer. This would create enough backlash in the system to eliminate most if not all of our actuator output motion.

MEMS research conducted at BYU [7] has addressed the topic of how to create free pin joints using MUMPS. A ring/disk structure is used in which one link is fixed to an outer ring while the other link is fixed to an inner disk. The fixed points prevent vertical motion. While this addresses our first concern, we are still faced with the minimum spacing design rule. This rule essentially negated the use of pin joints in the actuator connections. As a result, the actuator connecting rods are fixed to the lever. This is going to create some minor torsion and bending. This is an area that could cause some loss of performance in the design and will be investigated after the devices are fabricated.

In an attempt to minimize the impact of the fixed attachments, we tried to design the connecting rods based on a previous stepper motor design [8]. In this design, the connecting rods appeared to be 10-30 μm wide and about 200-400 μm long. The rods that we used were about 20 μm wide and 250-275 μm long. The connecting point is a $40 \times 40 \mu\text{m}^2$ square pad.

Lever The lever itself is relatively simple in design. At one end is a fixed pin joint. This pin is about 40 μm in diameter. For a 5x driver amplification, we placed the input link at 100 μm from the pin, and the output link at 500 μm . Based on tooth size and structure spacing, we determined that an available travel range of 20 μm would be needed for the pusher. Therefore, for this lever, we placed the input at 50 μm from the pin and the output at 500 μm .

In addition, for the pusher, the end of the lever has a small protrusion. This protrusion is the contact point between the pusher and the drive pawl.

Slider The slider is divided into three main sections – two toothed sliding sections and a central fiber-supporting section. Also, there is a latch on the left side for the locking mechanism. This can be seen in Figure 9.

The two sliding sections are adapted from a slider design obtained from an MUMPS design file. The one major modification made to these pieces is the tooth size and spacing. The original teeth were designed for a rack and pinion setup with circular gears. Because we have a drive pawl with momen-

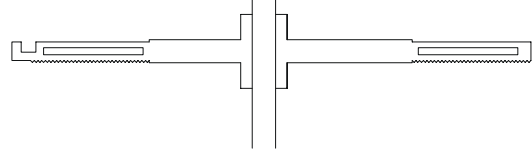


Figure 9. The slider.

tary contact, we modified the teeth to allow for more contact area.

We made the tooth spacing equal to the tooth size. We estimate that the drive pawl will move about 10 μm , so the teeth are spaced such that one push will advance the teeth by one position. A sketch of the teeth is shown in Figure 10. Tooth calculations are further discussed in the drive pawl section.

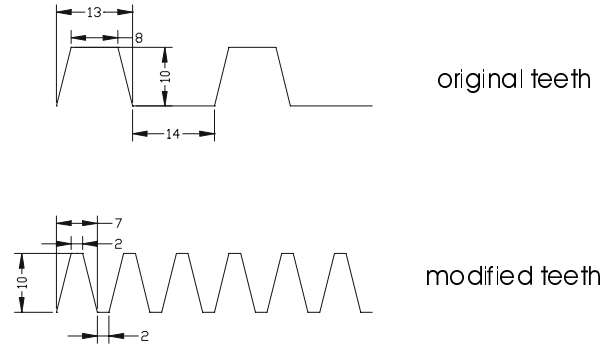


Figure 10. Tooth modifications.

Drive Pawl The toothed face of the drive pawl is 300 μm long. There are 32 teeth along this length. Assuming the best case where all teeth are in contact with the slider, the force per tooth is 14 μN (450 $\mu\text{N}/32$ teeth). For the worst case, all 450 μN are applied to one tooth. Looking at tooth shear stress for this worst case condition, we have

$$\tau = \frac{P}{A} = \frac{450\mu\text{N}}{7\mu\text{m} \cdot 2\mu\text{m}} \approx 32\text{MPa}. \quad (4)$$

Since the maximum allowable polysilicon shear stress is about 1 GPa, we should not have to worry about the drive teeth shearing during normal usage. Figure 11 shows a sketch of the drive pawl.

Latch The latch locks the slider into place in the second position. It is designed so that the switch can be at either position with no power being used by the system. Power is only required to make the switch move the fiber, but not hold it in place.

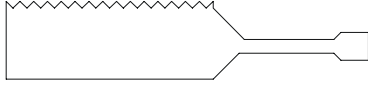


Figure 11. The drive pawl.

The lock is essentially a much longer lever. It rotates about a fixed pin, identical to the lever pin. (See Figure 12.)

The total length of the lock from the pin is $1625 \mu\text{m}$ with the input placed at $50 \mu\text{m}$. This will produce 32.5x motion amplification. An actuation of $2 \mu\text{m}$ will result in a $65 \mu\text{m}$ displacement of the latch end. The *hook* protrudes into the slider by $50 \mu\text{m}$. This allows for some clearance between the two pieces during motion.

The point on the latch that would fail first is most likely the pin. During the locked position, the force due to the bent fiber ($450 \mu\text{N}$) will be completely applied to the lock. Analyzing the shear on the pin, we have

$$\tau = \frac{P}{A} = \frac{450 \mu\text{N}}{\frac{\pi}{4} (40 \mu\text{m})^2} = 0.35 \text{MPa} \quad (5)$$

This is also well below the 1 GPa limit.

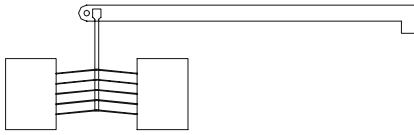


Figure 12. The latch.

5. Test Structures

The switch design only uses about 25% of the total available chip area, and there are 41 wire-bond pads unused. To use some of this extra space, we decided to develop some test structures that will help us refine future versions of the switch design.

We decided to develop tests to analyze the behavior of the bent-beam actuators that we are using. Of primary concern is the effect that different geometries will have on performance. To determine this, we designed bent-beam actuators with different angles to be tested for displacement and force output.

The following parameters are the same for each beam tested: $L = 400 \mu\text{m}$, $w = 4 \mu\text{m}$, and $t = 3.5 \mu\text{m}$.

The angles used for the test are: 0.5 rad, 1 rad, 2 rad, 3 rad, and 4 rad.

For each angle configuration, two beams were made, one for displacement measurements, and the other for force measurements.

5.1. Displacement Testing Beam

On the end of the first beam in each pair a micrometer is attached. Because we are not sure how well MUMPs can produce a fine micrometer, we put two scales with the pointer, as can be seen in Figure 13. The right scale has a mark every micrometer. The left scale is spaced wider, with a mark every two micrometers.

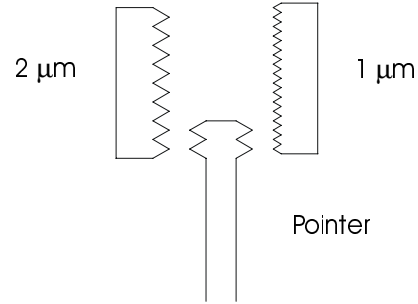


Figure 13. Micrometer.

5.2. Force Testing Beam

The second beam in each pair is connected to a force tester. This is essentially a cantilever beam with a displacement scale.

For ease in designing this tester, we used a beam similar to that used in modeling other MEMS actuators [9]. This force tester can be seen in Figure 14.

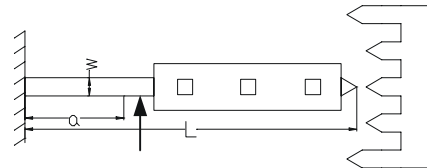


Figure 14. Force tester.

As the force is applied to a location before the pointer, the length a will deflect as a cantilever beam. This will be a small deflection. The pointer magnifies this because everything to the right of the force will be displaced according to the angle at the force point. The size and shape of the pointer does not affect beam bending in any way (neglecting mass). The deflection formula for this tester is

$$F = \left(\frac{Et w^3}{2(3a^2 L - a^3)} \right) d. \quad (6)$$

where d is the distance the pointer moves during deflection. For a much weaker actuator, typical values for the above equation are $t = 2 \mu\text{m}$, $a = 60 \mu\text{m}$, $L = 240 \mu\text{m}$, and $w = 2 \mu\text{m}$. Based on the actuator characteristics that we are using, the beam width and length must be modified to keep the deflection within an allowable range. We decided that because of the possible variations in the force output of the actuators, $d = 6 \mu\text{m}$ should indicate a force of $725 \mu\text{N}$. Keeping length the same, to obtain this relationship, $w = 12 \mu\text{m}$.

What we hope to obtain from these testers are behavioral curves for various bent-beam actuators. Primarily, these curves include (i) displacement vs current, (ii) force vs current, (iii) force vs displacement for different current levels. The different actuators could then be compared to determine the effect that geometry plays on performance. Displacement data was already collected for bent-beam actuators with different angles [6], but force data was not experimentally determined, thus leaving some important factors in actuator design unknown. Determining the behavior of these actuators could prove very beneficial to future designs.

6. Conclusion

MEMS-based optical switches are likely to be critical components in the design of fault-tolerant, reconfigurable, optical backplanes. Their potential for low cost and high data throughput are distinguishing characteristics compared to more traditional methods of optical switching. But to realize the potential of MEMS-based optical switching, numerous design questions need to be answered. In particular, switching optical fiber, the waveguide material of choice for low loss, requires large displacement and significant forces. Thermal actuators can accomplish, but the resulting structures are quite complex requiring displacement amplification and multiple actuators to achieve the necessary force. In this paper, we describe the design of a MEMS-based optical switch that uses a multiple thermal actuators in conjunction with a stepper motor. The switch is currently being fabricated by Cronos Integrated Microsystems.

Acknowledgment

This work was supported in part by Air Force (BMDO) contract F30602-98-C-0274, MinMAX Technologies, Inc., and Rowan University.

References

- [1] Wagner, R.E., Alferness, R.C., Saleh, A.A.M., Goodman, M.S., "MONET: Multiwavelength optical networking," *Jour. of Lightwave Technology*, **14**, 1349-1355 (1996).
- [2] Munoz, J. L., "Adaptive Computing Systems," *Proc. of DARPA Tech '97 - 19th Systems and Technology Symposium*, September (1997).
- [3] Congdom, P., "Microelectromechanical photonic switches," *DARPA/ETO*, <http://www.darpa.mil/MTO/MEMS/Projects/97MEMS/Texas-44.html>.
- [4] Kaiser, W., "Manufacturable microactuators and sensors," *DARPA/ETO*, <http://www.darpa.mil/MTO/MEMS/Projects/97MEMS/University-54.html>.
- [5] Lau, K. and Muller, R., "Adaptive microelectromechanical technologies for optoelectronic modules and systems," *DARPA/ETO*, <http://www.darpa.mil/MTO/MEMS/Projects/97MEMS/University-48.html>.
- [6] Que, L., Park, J.-S., and Gianchandani, Y.B. "Bent-Beam Electro-Thermal Actuators for High Force Applications," *Proc. 12th Annual International Conference on Micro Electro Mechanical Systems*, Orlando, FL (1999).
- [7] BYU. Pin Joints. Pin Joints at BYU. http://www2.et.byu.edu/~llhwww/current_research/pin_joint/pinjoint.html July (1998).
- [8] Bright, V.M., et al., "Realizing micro-opto-electromechanical devices through a commercial surface-micromachining process," in *Miniturized Systems with Micro-Optics and Micromechanics*, M. Edward Motamedi, Editor, Proc. SPIE **2687**, 34-46 (1996).
- [9] Reid, R.J., Bright, V.M., Comtois, J.H., "Force measurements of polysilicon thermal microactuators," in *Micromachined Devices and Components II*, Kevin Chau, Pay M. Roop, Editors, Proc. SPIE **2882**, 296-306 (1996).